Experimental results of nonlinear structure coupled through nonlinear connecting elements

F. Latini [1], **J. Brunetti** [2], **M. Kwarta** [3], **M. S. Allen** [3], **W. D'Ambrogio** [2], **A. Fregolent** [1]

[1] Università di Roma La Sapienza, Dipartimento di Ingegneria Meccanica e Aerospaziale,
Via Eudossiana 18, 00184 Rome, Italy
e-mail: **francesco.latini@uniroma1.it**

[2] Università dell'Aquila, Dipartimento di Ingegneria Industriale e dell'Informazione e di Economia,
Via G. Gronchi 18, 67100 L'Aquila (AQ), Italy

[3] University of Wisconsin-Madison, Department of Engineering Physics,
534 Engineering Research Building, 1500 Engineering Drive, Madison, WI 53706, USA

Abstract

In many complex engineering systems, significant nonlinear effects can be ascribed to the connections between coupled subsystems. For this reason, when analyzing the dynamics of the coupled assembly it is possible to assume that the subsystems behave linearly and that the nonlinear effects are only due to the connections. In order to analyze this possible scenario, an experimental setup is developed. It is composed of two linear beams coupled through two nonlinear connecting elements. Measurements are performed on each component of the assembly to build the corresponding linear and nonlinear numerical models. Experimental tests are also performed on the coupled system to obtain its nonlinear normal modes and compare them to the numerical results obtained from a nonlinear substructuring procedure in the modal domain.

1   Introduction

Many systems in nature are nonlinear, thus when dynamic analyses are performed it is often necessary to include the nonlinearities to obtain accurate results. In some engineering scenarios, the most relevant nonlinear effects are due the connections between coupled subsystems, as it happens with bolted joints [1] and wire rope isolators [2]. In these cases, it is possible to neglect the nonlinearities of the connected subsystems and account only for the nonlinearity of the connections. One possible way to analyze the effects of nonlinear phenomena occurring in a system is by computing its Nonlinear Normal Modes (NNMs).

NNMs represent an extension of Linear Normal Modes for nonlinear systems [3], and are defined as the "non-necessarily synchronous periodic motion of a conservative nonlinear system" [4]. They can be computed using different methods: shooting and pseudo-arclength continuation [5], Harmonic Balance (HB) [6] and Modal Derivatives (MDs) [7], to name a few. Besides, different procedures have been proposed to measure the NNMs of a structure [8, 9].

This work aims at analyzing the dynamic behavior of an experimental setup composed of two beams connected through two Nonlinear Connecting Elements (NLCEs). This assembly has been designed at the University of Wisconsin-Madison in order to have a system whose main nonlinear effects are due to the presence of the NLCEs. In fact, the NLCEs are specifically designed to have a nearly cubic nonlinear behavior such that the beams can be assumed to behave linearly. Experimental tests are performed on each subsystem to characterize its dynamics. For the beams, since they can be considered as linear, FRFs alone allow to identify their dynamics in terms of resonance frequencies. In contrast, each NLCE is tested in order to measure its NNMs by performing the experimental procedure proposed by Peeters et al. [9] and by Ehrhardt et al. [8]. Also, the dynamic behavior of the complete assembly is evaluated and one of its NNMs is measured.

The measurement campaign on the components of the assembly provides the experimental data that are used as reference to build the linear and nonlinear numerical models of the beams and of the NLCEs, respectively. These models can then be used to perform substructuring analyses and build the model of the complete assembly to retrieve its nonlinear dynamic behavior. Dynamics Substructuring approaches [10] are very useful since they allow to tackle problems either in physical [11], modal [12] and frequency [13] domains, enabling the use different types of models, either numerical [14] and experimental [15, 16]. These techniques can be applied to different cases: the dynamic behavior of complex systems can be obtained starting from the known dynamic behavior of its component substructures (coupling) [17]; also, it is possible to obtain the behavior of one substructure from the known behavior of the complete structure and that of the residual substructures (decoupling) [18, 19]. However, substructuring techniques are based on the assumption that the component substructures are linear. This represents a strong limitation when the considered subsystems are known to behave nonlinearly [20]. Thus, nonlinear effects must be included in the analyses if accurate results are needed.

Different attempts have been made to include the nonlinearities in the substructuring procedure. Chong and Imregun [21] suggest two different approaches named construction and extraction to model the behavior of the nonlinear substructures and proceed with the coupling in the modal domain. Kalaycioğlu et al. propose an iterative frequency-based approach based on the method introduced by Özgüven in [22] to deal with structural modifications for linear systems. In particular, in [23] the nonlinear FRFs of a coupled system are computed using those of the original system and the dynamic stiffness matrix of the nonlinear modifying system. Hughes et al. [24] developed an interface reduction technique on a nonlinear model in which two beams are bolted together at each end in order to decrease the computational time and obtain highly reliable results. Andersson et al. [25] analyze the effects that nonlinearities at the interface between substructure have on the dynamics of the assembly by reducing each subsystem with component mode synthesis. The nonlinear coupling procedure in the modal domain, outlined in [26, 27] and inspired by the work of Kuether and Allen [28], is used to obtain the NNMs of the coupled assembly. The experimental results on the assembled system are then compared to the numerical results provided by the nonlinear coupling procedure, in order to assess the accuracy of the method.

In Section 2 the experimental setup is presented, along with the mechanical properties of the single components. In Section 3 the test procedure for each component is described and the identification process is outlined. In Section 4 the results for the complete assembly are presented and the comparison between the numerical and experimental results is provided.

2   Experimental Setup

The measurement campaign is performed on the the assembly shown in Figure 1(a). It is composed of two beams of 910 mm x 30 mm x 6.35 mm made of steel, connected together through two Nonlinear Connecting Elements (NLCEs). Since the system is hung from the frame through bungees, it can be considered as unconstrained.

The most important element of this system is the NLCE, shown in Figure 2(a). It has to be significantly nonlinear such that the nonlinearities of the beams can be neglected and they can be assumed to behave linearly. The NLCE is composed of a C-shaped element and a T-shaped element, connected together by a thin plate made of spring steel, as shown in Figure 2. The NLCE dimensions are listed in Table 1. The nonlinear behavior of the NLCE depends on the nonlinearity introduced by a thin plate clamped at both ends which experiences a large displacement at mid-span, similarly to the case of a beam clamped at one end in [23]. Experimental tests are performed on each component of the assembled structure in order to build the corresponding numerical models that fit the experimental data. Once the properties of either linear substructures and the NLCEs are identified, the whole system can be modeled in Matlab. The beams are modeled using 65 Euler-Bernoulli finite elements of equal length, as shown in Figure 1(b). Every node has two degrees of freedom, the one related to the vertical displacement and the one accounting for the rotation. The NLCEs are modeled as a nonlinear cubic springs (orange lines) and are placed in accordance with their position in the real assembly.

Table 1: Dimensions of the NLCE

b	d	h_{up}	h_{down}	l	w	t_b	t_p	
12	57	20	15	150	30	5	0.2	[mm]

3   Experimental characterization of components

The dynamics of each component is experimentally analyzed in order to have reference data to build the corresponding numerical models. Since the beams can be assumed to behave linearly, their FRFs are experimentally evaluated to identify the resonance frequencies. On the other hand, the nonlinear behavior of each NLCE needs to be investigated through a more sophisticated analysis, that involves the measurement of their response at several excitation levels.

3.1   Experimental Tuning of Beam Models

The FRFs are evaluated for each beam to have an estimate of their resonance frequencies. Tests are performed by applying a burst random excitation using a shaker (Modal Exciter 2100E11), measuring the response through a laser vibrometer (Polytec PSV 400) and the applied force through a piezoelectric force sensor (PCB 208C04). Figure 3 shows in blue the drive point FRF measured on one beam, where four different resonance frequencies are found in the range between 0 and 500 Hz.

Their geometric dimensions and the weight are known, thus it is possible to adjust the value of the Young Modulus such that the resonance frequencies of the numerical model match the measured ones. Using the Euler-Bernoulli theory, the expression of the i-th resonance frequency for the beam is:

$$\omega_i = k_i^2 \sqrt{\frac{EI}{\rho A}} \tag{1}$$

where I is the moment of inertia, A is the area of the section, E is the Young Modulus, ρ is the density and k_i is the wavenumber. This last term, for the case of a beam unconstrained at both ends, can be found by solving:

$$\cos(k_i l)\cosh(k_i l) = 1 \tag{2}$$

The value of Young Modulus can then be evaluated for each measured resonance frequency by solving Eq. 1. Averaging the results it is possible to find that $E \approx 214$ Gpa. The comparison between the numerical and experimental FRFs of the upper beam is shown in Figure 3.
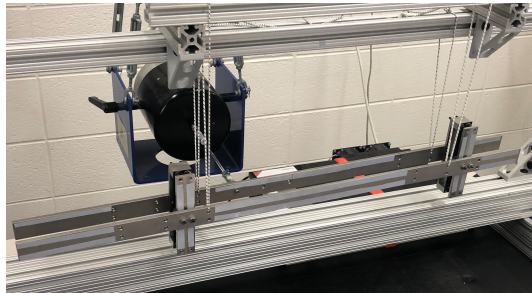
(a) Assembled System.
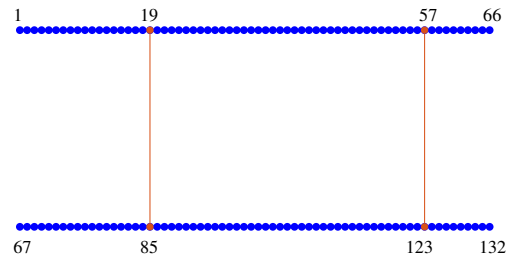
(b) Structure of the unconstrained system. The horizontal lines represent the linear beams, the two vertical lines represent the two NLCEs.

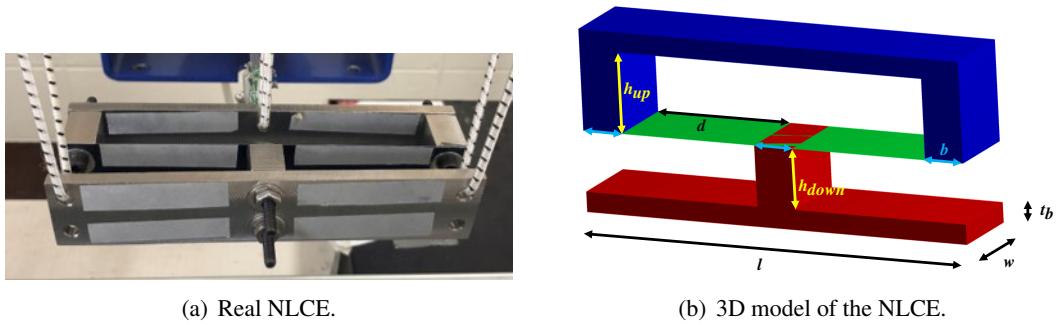Figure 1: Experimental setup, composed of two beams connected through two NLCEs.

(a) Real NLCE.

(b) 3D model of the NLCE.
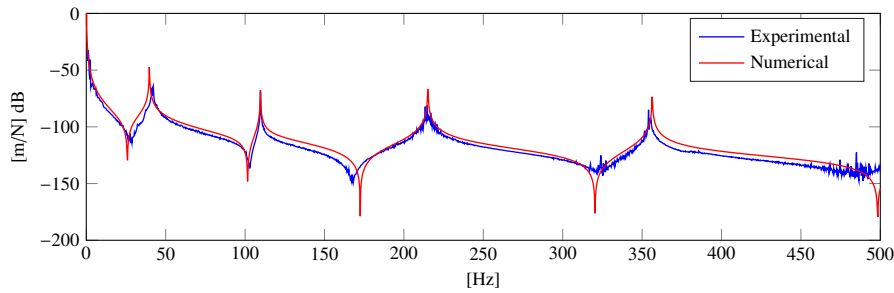
Figure 2: Nonlinear connecting element.

Figure 3: Comparison between the numerical and experimental FRF of one beam.

3.2 Experimental Identification of the Nonlinear Connecting Element

Each NLCE is considered as a substructure during the substructuring procedure [26], thus it is necessary to measure their NNMs. After having measured the NNMs of interest, they are used as reference to find the coefficients of the cubic law that suitably approximates the NLCEs' behavior. The whole experimental procedure to obtain the NNM is here explained and partial results are shown for the left NLCE (Figure 1(a)); the same procedure is applied also to the right NLCE. As first, the response to a low amplitude burst random excitation is measured using a laser scanner vibrometer to estimate the linear frequency corresponding to the mode of interest, which is around 43 Hz. The set of measurement points is shown in Figure 4, where points on red lines (1-20) refer to the T-shaped element, points on the blue line (21-30) to the thin plate and points on the green lines (31-40) to the C-shaped element.

Being the resonance frequency of a NNM dependent on the energy, it is identified for different levels of excitation. For a given amplitude, the frequency of the sinusoidal excitation is adjusted to attain the resonance condition: i.e. the velocity measured by the scanner and the input signal are in-phase or 180° out-of-phase [8,
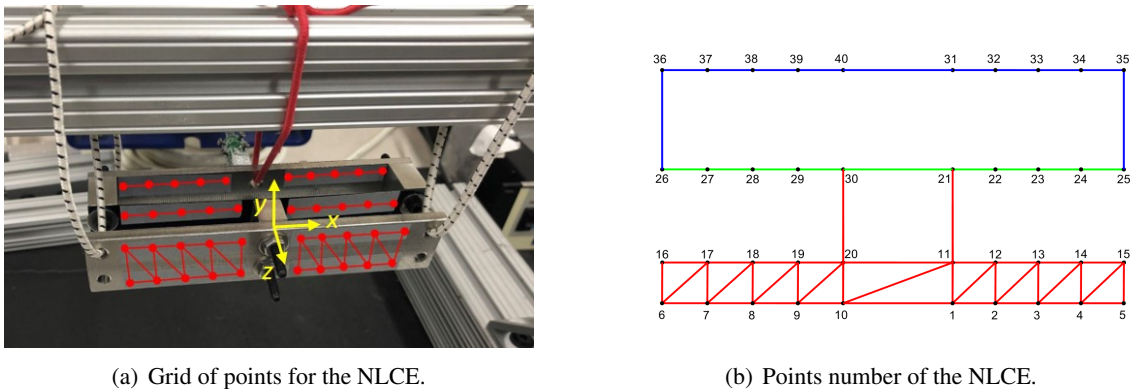
(a) Grid of points for the NLCE.

(b) Points number of the NLCE.

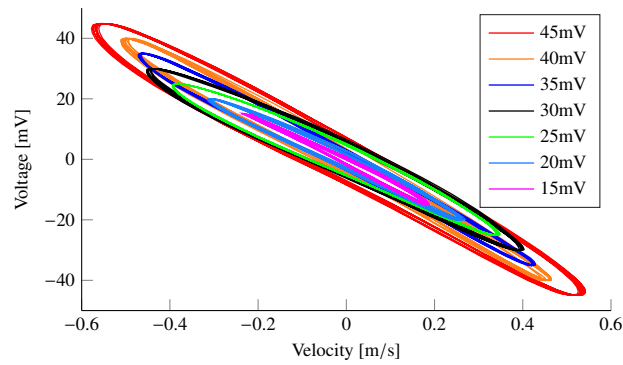Figure 4: Set of measurement points for the NLCE.

Figure 5: Resonance condition in which the measured velocity of point 11 is almost 180° out-of-phase with respect to the input signal at the 7 excitation levels.

9]. This procedure is performed for seven increasing levels of excitation for each NLCE. Once the resonance condition is attained, the velocity of oscillation of each measurement point is recorded for a time interval of 0.2 s (corresponding to 8 periods of oscillation at 40 Hz) and the amplitude-frequency pair of the excitation are stored. Figure 5 shows the resonance condition for a point of the T-shaped element (point 11) at the seven excitation levels. It is possible to see that all the curves have a similar shape, and that the velocity signal is as close as possible to be 180° out-of-phase with respect to the voltage input (particularly evident for the excitation at 15 mV). For high excitation levels, the non perfect overlapping is due to the practical difficulty in getting close to the resonance condition without falling off the NNM branch. The integration of the velocity signal leads to the displacement time series for the points of the C and T shaped elements. Figure 6 shows the velocity and displacement signals for point 1. A high-pass Butterworth filter with a low cut-off frequency of 20 Hz is used to remove the low frequency contents from the velocity signal due to the presence of the bungees (red curve in Figure 6(a)). The filtered signal (blue curve in Figure 6(a)) is subjected to distortion in amplitude up to the second peak of oscillation ($\approx$ 0.04 s), thus that part is neglected for the further steps of the procedure.
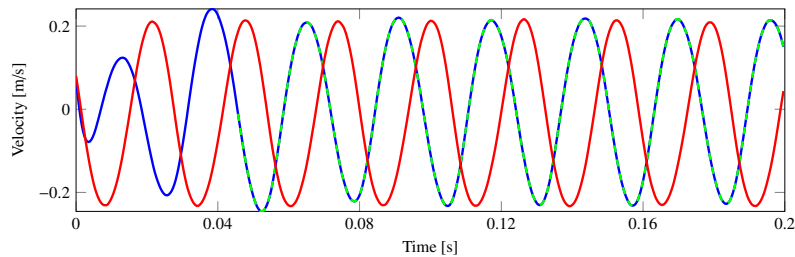

(a) — measured response; — measured response after filter application; - - part of the signal used for the NNM determination.
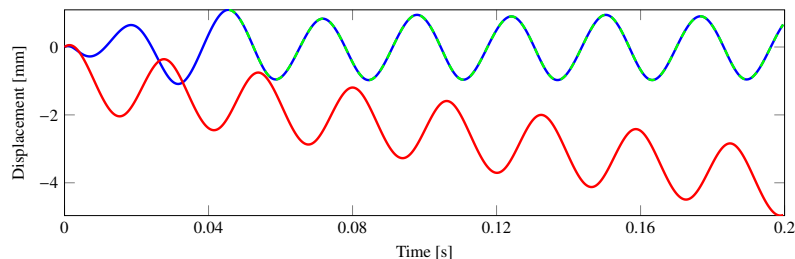

(b) — integrated measured response; — integrated filtered signal; - - integrated part of the signal used for the NNM determination.

Figure 6: Raw and high pass (AC) filtered velocity and displacement signals for node 1.

Although there is phase shift introduced by the filter, all the responses are almost harmonic at the same
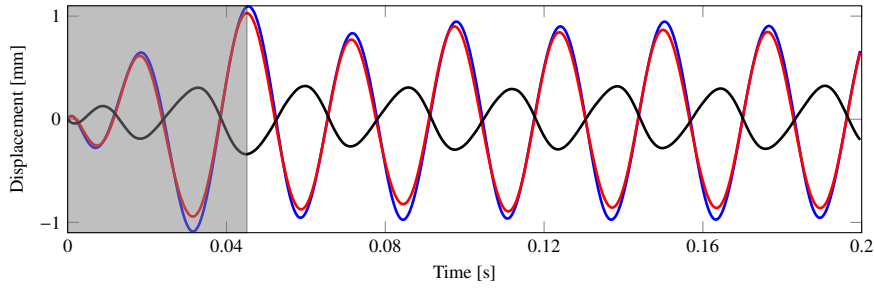
(a) Displacement signals for: — Node 1; — Node 11; — Node 31. The gray rectangle highlights the part of the signal that is not used for the reconstruction of the NNM.
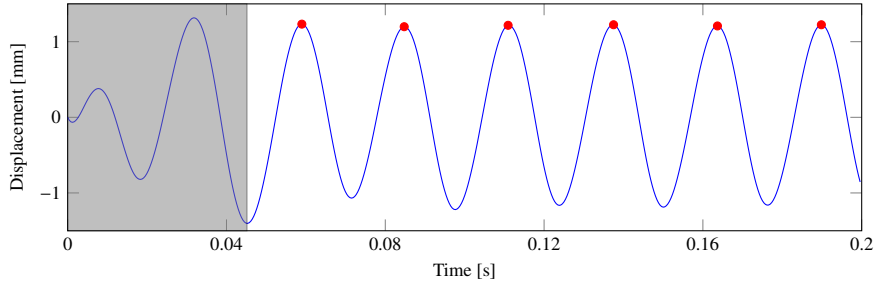
(b) Relative displacement between set of nodes $(n_{31}, n_1 - n_{11})$.

Figure 7: Oscillation signals for $(n_{31}, n_1 - n_{11})$.

frequency, thus the change in phase that they experience is the same. Considering the NLCE as two masses connected by a cubic spring, its resonance frequency can be associated with the amplitude of the relative displacement between the C-shaped and T-shaped elements. In Figure 6(b) it is shown the difference between the displacement signals obtained before and after the filtering (red and blue curve, respectively). It is evident that it is not possible to use the velocity signal as measured from the vibrometer since, being its average value different from zero, when it is integrated it leads to a signal drift that would give erroneous results, thus the green part of the filtered signal is used. For each of the ten values of abscissa, one point on the C-shaped and two points on the T-shaped element are present: for instance, referring to Figure 4, one set of nodes is $(n_{31}, n_1 - n_{11})$. The displacement signals for nodes $(n_{31}, n_1 - n_{11})$ are shown in Figure 7(a).

The responses for the two points belonging to the T-shaped element (points 1 and 11) almost coincide; the small difference highlights a small rotation of the T-shaped element along the x direction (see Figure 4(a)). Besides, it is possible to see that those responses are $180°$ out of phase with respect to the one of the point belonging to the C-shaped element (point 31). For the NNM searched it is expected since this is the configuration that leads to the maximum deformation of the nonlinear element. The frequency of oscillation for a given excitation level is obtained by averaging the frequencies estimated by fitting the filtered velocity signal with a sinusoidal function for each point. The amplitude of the NNM is obtained performing these steps:

Step 1: The displacement responses of pairs of points sharing the same abscissa and belonging to the T-shaped element are averaged to cancel out the rotational effect (for instance, $(u_1 + u_{11})/2$);

Step 2: The relative displacement between the point belonging to the C-shaped element and the points belonging to the T-shaped element (response obtained from Step 1) is computed for each abscissa value;

Step 3: The amplitude of oscillation is estimated by averaging the value of the relative maximum points over the portion of the signal selected after the filtering (Figure 7(b)).

These steps are performed for every group of 3 nodes and for every level of excitation (seven in total), resulting in ten curves, each one containing seven points corresponding to the measured data. The amplitude of the NNM is obtained for the two NLCEs by averaging the results of the ten set of points, as shown in
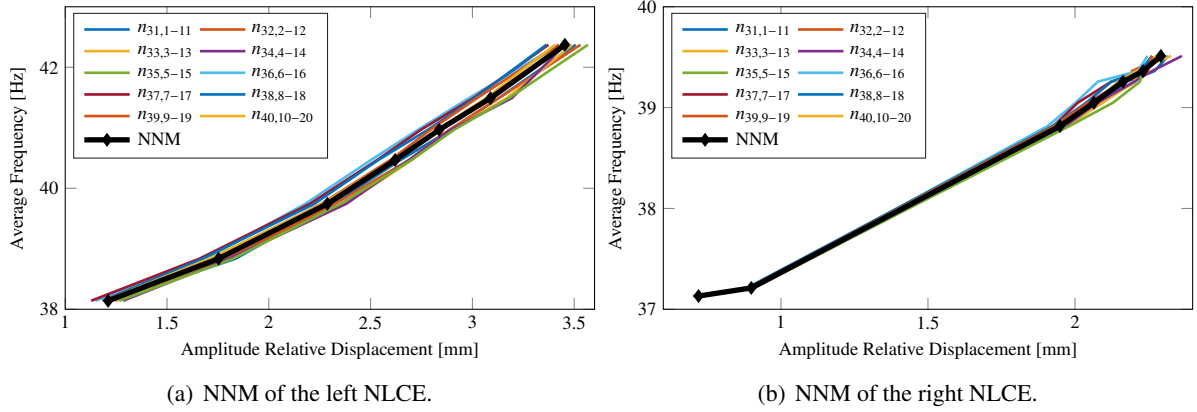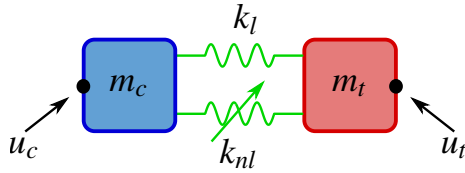
(a) NNM of the left NLCE.

(b) NNM of the right NLCE.

Figure 8: NNMs of the two NLCEs.

	k_l [N/m]	k_{nl} [N/m^3]
Left Spring	7180	1.73×10^9
Right Spring	6978	2.04×10^9

Figure 9: Model of the NLCE (left) and coefficients of the cubic law for the two springs (right).

Figure 8. The two curves show that both the NLCEs experience an hardening behavior. In particular, for the right NLCE, in the range between 37.2 Hz and 38.8 Hz there are not available data since the resonance condition was difficult to maintain. The objective is to model the NLCE as a nonlinear substructure in which two masses, representative of the T-shaped and C-shaped elements, are connected through a cubic spring. It is then necessary to find the correct values for the parameters k_l and k_{nl} of the cubic law such that the numerical NNM retraces the experimental one. The linear angular frequency of the out-of-phase mode for such a system is equal to:

$$\omega_n = \sqrt{\frac{k_l}{m_{eq}}} \quad \text{with} \quad m_{eq} = \frac{m_t m_c}{m_t + m_c} \tag{3}$$

where m_t and m_c are the masses of the T-shaped and C-shaped element, respectively, as shown in the left side of Figure 9. Thus, assuming the mode of interest to be the one of a Duffing oscillator with mass m_{eq} and linear and nonlinear spring k_l and k_{nl}, the resonance angular frequency is expressed as function of the amplitude A as [29]:

$$\omega_r = \sqrt{\omega_n^2 + \frac{3k_{nl}}{4}A^2} \tag{4}$$

Hence, the parameters k_l and k_{nl} are estimated by performing a minimization through a least-square error method, using the experimental results as reference. The resulting coefficients are shown in the right side of Figure 9. Figure 10 shows that the numerical NNMs are in good agreement with the experimental ones. However, for the right NLCE, the absence of data in the range between 37.2 Hz and 38.8 Hz (see Figure 8(b)) might affect the accuracy of the obtained parameters. Also, it is worth remarking that the simplified 2DoFs model does not take into account rotational DoFs since the effect of the longitudinal spring alone is considered.

4 Experimental nonlinear behavior of the assembly

The dynamic response of the assembled system in the free-free configuration is analyzed in order to measure one of its NNMs. The objective is to compare the numerical result obtained performing the Coupling Proce-
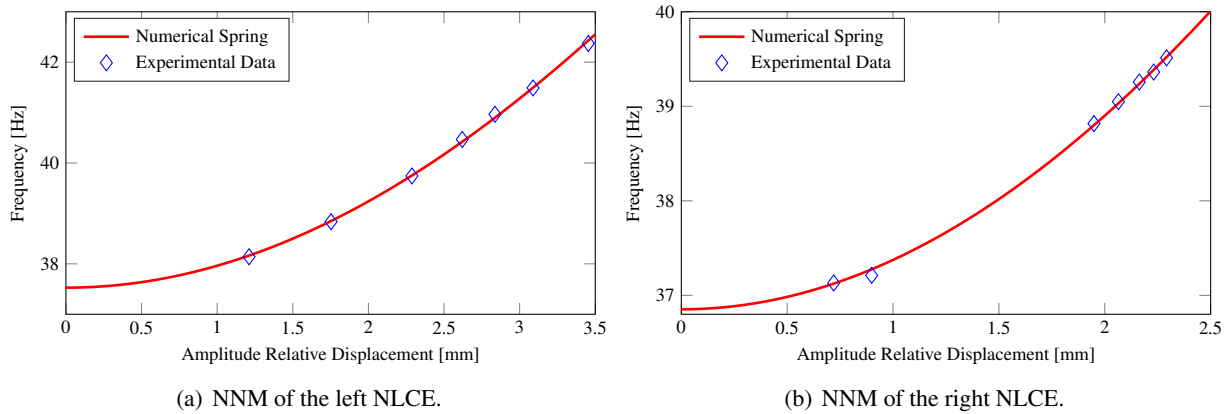
(a) NNM of the left NLCE.

(b) NNM of the right NLCE.

Figure 10: Comparison of the numerical and experimental NNMs.

dure (CP) described in [26] to the experimental ones. The measurement procedure aims at identifying both the resonance frequency and the mode shape of the system at different excitation levels. The experimental response of a set of points is measured through the scanner laser vibrometer with an excitation provided by the shaker, as previously shown in Figure 1(a). Figure 11 shows the set of measurement points for the lower beam and the NLCEs; the measurement points on the upper beam are not visible from this view. The measurement of the NNMs for the unconstrained assembled system is performed as for the NLCEs by setting the amplitude and by adjusting the frequency of the harmonic excitation to identify the resonance conditions. Since the linear frequency of the mode of interest is at 41 Hz, the velocity signal of each point is filtered using a high pass Butterworth filter with a low cut-off frequency of 20 Hz and then integrated to obtain the displacement response, as for the NLCE. Figure 12 shows a resonance condition at a given excitation level for a subset of measurement points for the two beams and the two NLCEs. For some points the velocity is in-phase with the voltage input, for others the signals are 180° out-of-phase. This gives an insight of the mode shape of the beams at the considered excitation level. For each excitation level (i.e. fixed pair of amplitude and frequency of the sinusoidal input), the amplitude and phase of oscillation are identified and polynomial functions are used to fit the mode shape of the assembled system. Figure 13 shows the mode shapes of the system at each excitation level. It is possible to see that the nodal points move as the excitation increases (from blue to red curves), thus leading to a change in the mode shapes. In particular, it is worth noticing that the right NLCE is much more deformed than the left one.

Once the NNM of the system is measured, it is possible to compare it with the results obtained by coupling the models of the beams through the NLCEs, assuming a rigid connection between the pairs of matching DoFs. However, it is not possible to compare the numerical and experimental NNMs by using the FEP diagram because the measured data cannot be expressed as function of the total mechanical energy of the system, as it is done numerically. In fact, for excitation level, the experimental results of the NNM are expressed in terms of the resonance frequency and the amplitude of oscillation of the measurement points.

In this particular case, it is possible to express the resonance frequency of the NNM as function of the deformation of the right NLCE that is the nonlinear component experiencing the highest deformation. The experimental results are compared in Figure 14(a) to the numerical results obtained by coupling the the updated beams (Section 3.1) and the identified NLCEs (Section 3.2) using the numerical procedure outlined
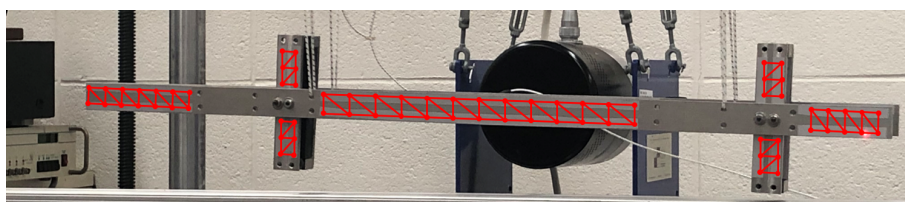

Figure 11: Grid of measurements points on the bottom beam and on the NLCEs of the assembly.
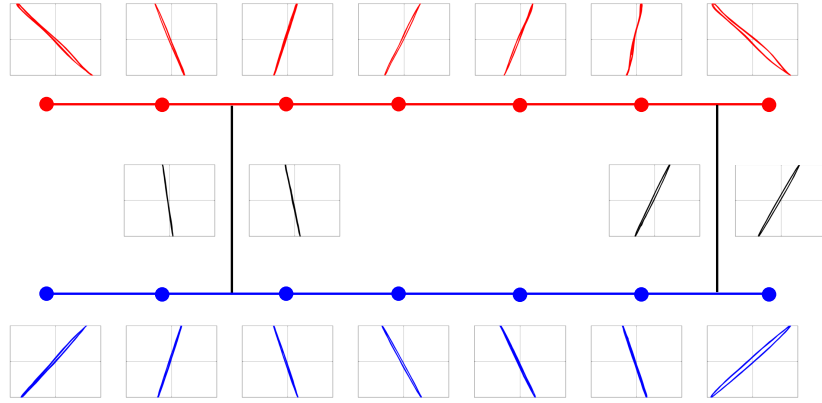
Figure 12: Resonance condition on a subset of measurement points of the assembly. For each point the plot shows the voltage input vs the velocity. All the plots have the same x and y axis scales.
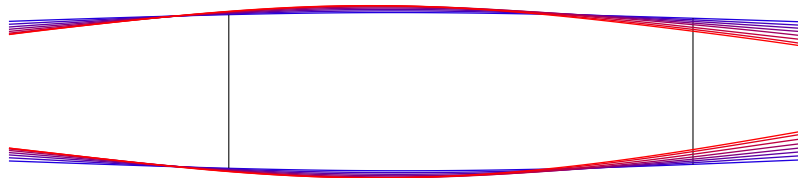

Figure 13: Mode shape comparison from low amplitude excitation (blue curves) to high amplitude excitation (red curves).

in [26]. Using the models based on the experimental identification it is possible to see that there is an increasing error as the deformation of the right NLCE grows. However, there is a good correlation between the experimental and numerical mode shapes, as shown by the MAC value in Figure 14(b), which is almost unitary up to a deformation of the right spring of 2.51 mm and it decreases to 0.91 at 4.35 mm. In particular, the best correlation is achieved for values of deformation of the right spring inside the range for which its parameters (k_l and k_{nl}) are experimentally evaluated (Figure 10(b)).

Besides, an optimization of the parameters for both the NLCEs is carried out to investigate the causes of the error in frequency highlighted in Figure 14(a). Although the beams and NLCEs are singularly experimentally identified, the real connection is not perfectly rigid, as it is assumed in the numerical model. Also, the error in frequency could be due to the lack in accuracy on the estimation of the coefficients of the cubic law for the right NLCE. In fact, as seen from Figure 14, the right NLCE experiences a deformation that is partially in the range where there are no data for the identification (from 0.89 mm to 1.9 mm) and partially in a range where the behavior of the NLCE is extrapolated over 2.23 mm. Thus, the optimization aims at finding the linear and nonlinear parameters of the NLCEs' that account also for the non-modeled local effects of the real interface. A multi-objective optimization technique is performed to simultaneously minimize the differences between the numerical frequencies and the experimental ones for each excitation level. The frequency-deformation curve obtained by using the optimized coefficients (Table 2) are shown in Figure 14(a). The optimized coefficients for each NLCE, especially for the right one, are lower than the ones experimentally identified. This may be explained if considering an additional flexibility of the connection between the beams and the NLCE. The different behavior between the two NLCEs can be either incidental or due to the unequal amplitude of vibration of the two NLCEs, thus leading to different loosening of the connections. The frequency-deformation plot obtained using the optimized parameters almost overlaps on the experimental one with an average error in frequency of $\approx 0.41\%$. However, using the optimized parameters instead of
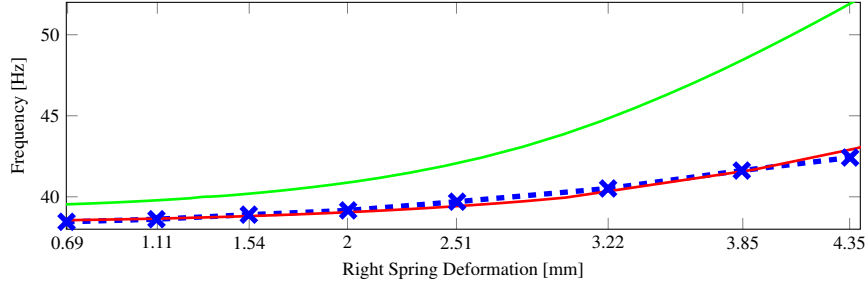
(a) Frequency Deformation Plot: **-x-** experimental; **—** CP with experimentally identified NLCEs parameters; **—** CP with optimized NLCEs parameters.
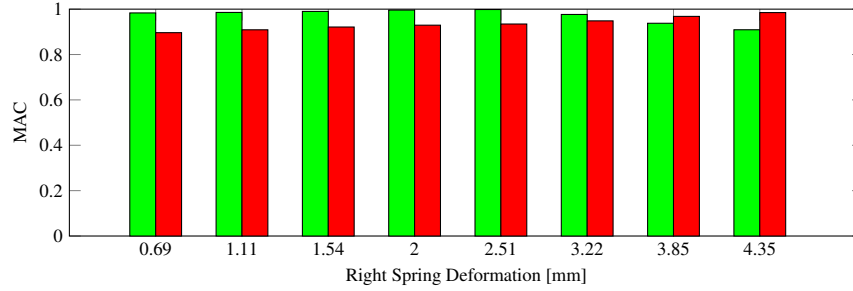
(b) MAC between numerical and experimental results: ■ using results from CP with experimentally identified NLCEs parameters; ■ using results from CP with optimized NLCEs parameters.

Figure 14: Comparison between experimental results and two sets of numerical results.

Table 2: Coefficients of the cubic law for the two NLCEs after optimization.

	k_l [N/m]	k_{nl} [N/m^3]
Left NLCE	4000	1.6×10^9
Right NLCE	2000	1.2×10^9

the identified ones, the correlation between the experimental and numerical mode shapes decreases slightly below 3.22 mm and it improves at 3.85 mm and 4.35 mm (Figure 14(b)).

5 Concluding remarks

The design of the experimental assembly proved to be valid in order to measure NNMs due to the presence of nonlinearities localized at the connection between two linear subsystems. The nonlinear hardening behavior of the specifically designed NLCEs has been successfully measured using an experimental procedure able to track the resonance condition at different excitation levels. One NNM of the complete assembly is identified and the evolution of the mode shapes of the complete system for the different excitation levels is well captured. Experimental results are compared to the numerical results obtained via a nonlinear substructuring procedure. A coherent variation of the resonance frequency as function of the excitation level is obtained, and a good correlation between the mode shapes is found. Eventually, a multi-objective optimization is performed to improve the numerical model providing information about the causes of the error in frequency.

Acknowledgements

References

[1] R. Lacayo, L. Pesaresi, J. Groß, D. Fochler, J. Armand, L. Salles, C. Schwingshackl, M. Allen, and M. Brake, "Nonlinear modeling of structures with bolted joints: a comparison of two approaches based on a time-domain and frequency-domain solver," *Mechanical Systems and Signal Processing*, vol. 114, pp. 413–438, 2019.

[2] P. S. Balaji, M. E. Rahman, L. Moussa, and H. H. Lau, "Wire rope isolators for vibration isolation of equipment and structures–A review," in *IOP Conference Series: Materials Science and Engineering*, vol. 78, no. 1. IOP Publishing, 2015, p. 012001.

[3] R. M. Rosenberg, "Normal modes of nonlinear dual-mode systems," 1960.

[4] G. Kerschen, M. Peeters, J. Golinval, and A. F. Vakakis, "Nonlinear normal modes, Part I: A useful framework for the structural dynamicist," *Mechanical Systems and Signal Processing*, vol. 23, no. 1, pp. 170–194, 2009.

[5] M. Peeters, R. Viguié, G. Sérandour, G. Kerschen, and J. Golinval, "Nonlinear normal modes, Part II: Toward a practical computation using numerical continuation techniques," *Mechanical systems and signal processing*, vol. 23, no. 1, pp. 195–216, 2009.

[6] M. Krack and J. Gross, *Harmonic balance for nonlinear vibration problems*. Springer, 2019.

[7] C. Sombroek, L. Renson, P. Tiso, and G. Kerschen, "Bridging the gap between nonlinear normal modes and modal derivatives," in *Nonlinear Dynamics, Volume 1*. Springer, 2016, pp. 349–361.

[8] D. A. Ehrhardt, M. S. Allen, and T. J. Beberniss, "Measurement of Nonlinear Normal Modes using Mono-harmonic Force Appropriation: Experimental Investigation," in *Nonlinear Dynamics, Volume 1*. Springer, 2016, pp. 241–254.

[9] M. Peeters, G. Kerschen, and J.-C. Golinval, "Dynamic testing of nonlinear vibrating structures using nonlinear normal modes," *Journal of Sound and Vibration*, vol. 330, no. 3, pp. 486–509, 2011.

[10] D. de Klerk, D. J. Rixen, and S. N. Voormeeren, "General Framework for Dynamic Substructuring: History, Review, and Classification of Techniques," *AIAA journal*, vol. 46, no. 5, 2008.

[11] D. J. Rixen, "A dual Craig-Bampton method for dynamic substructuring," *Journal of Computational and applied mathematics*, vol. 168, no. 1-2, pp. 383–391, 2004.

[12] R. L. Mayes, P. Hunter, T. W. Simmermacher, and M. S. Allen, "Combining experimental and analytical substructures with multiple connections." Sandia National Lab.(SNL-NM), Albuquerque, NM (United States), Tech. Rep., 2007.

[13] B. Jetmundsen, R. L. Bielawa, and W. G. Flannelly, "Generalized frequency domain substructure synthesis," *Journal of the American Helicopter Society*, vol. 33, no. 1, pp. 55–64, 1988.

[14] J. Brunetti, A. Culla, W. D'Ambrogio, and A. Fregolent, "Selection of interface dofs in hub-blade(s) coupling of ampair wind turbine test bed," vol. 2, 2014, pp. 167–178.

[15] M. S. Allen, R. L. Mayes, and E. J. Bergman, "Experimental modal substructuring to couple and uncouple substructures with flexible fixtures and multi-point connections," *Journal of Sound and Vibration*, vol. 329, no. 23, pp. 4891–4906, 2010.

[16] J. Brunetti, A. Culla, W. D'Ambrogio, and A. Fregolent, "Experimental dynamic substructuring of the Ampair wind turbine test bed," vol. 1, 2014, pp. 15–26.

[17] R. Craig, Jr, "Coupling of substructures for dynamic analyses-an overview," in *41st Structures, Structural Dynamics, and Materials Conference and Exhibit*, 2000, p. 1573.

[18] S. N. Voormeeren and D. J. Rixen, "A family of substructure decoupling techniques based on a dual assembly approach," *Mechanical Systems and Signal Processing*, vol. 27, pp. 379–396, 2012.

[19] W. D'Ambrogio and A. Fregolent, "Decoupling procedures in the general framework of frequency based substructuring," *Proceedings of 27th IMAC. Orlando (USA)*, 2009.

[20] D. Roettgen, B. Pacini, and B. Moldenhauer, "How Linear Is a Linear System?" in *Topics in Modal Analysis & Testing, Volume 8*. Springer, 2020, pp. 185–192.

[21] Y. H. Chong and M. Imregun, "Coupling of non-linear substructures using variable modal parameters," *Mechanical Systems and Signal Processing*, vol. 14, no. 5, pp. 731–746, 2000.

[22] H. N. Özgüven, "Structural modifications using frequency response functions," *Mechanical Systems and Signal Processing*, vol. 4, no. 1, pp. 53–63, 1990.

[23] T. Kalaycıoğlu and H. N. Özgüven, "Nonlinear structural modification and nonlinear coupling," *Mechanical Systems and Signal Processing*, vol. 46, no. 2, pp. 289–306, 2014.

[24] P. J. Hughes, W. Scott, W. Wu, R. J. Kuether, M. S. Allen, and P. Tiso, "Interface reduction on hurty/craig-bampton substructures with frictionless contact," in *Nonlinear Dynamics, Volume 1*. Springer, 2019, pp. 1–16.

[25] L. Andersson, P. Persson, P. E. Austrell, and K. Persson, "Reduced order modeling for the dynamic analysis of structures with nonlinear interfaces," in *7th International Conference on Computational Methods in Structural Dynamics and Earthquake Engineering, COMPDYN 2019*, vol. 2. National Technical University of Athens, 2019, pp. 2395–2406.

[26] F. Latini, J. Brunetti, W. D'Ambrogio, and A. Fregolent, "Substructures' coupling with nonlinear connecting elements," *Nonlinear Dynamics*, pp. 1–16, 2019.

[27] J. Brunetti, W. D'ambrogio, A. Fregolent, and F. Latini, "Substructuring using nnms of nonlinear connecting elements," *Lecture Notes in Mechanical Engineering*, pp. 1426–1440, 2020.

[28] R. J. Kuether and M. S. Allen, "Nonlinear modal substructuring of systems with geometric nonlinearities," in *54th AIAA/ASME/ASCE/AHS/ASC Structures, Structural Dynamics, and Materials Conference*, 2013, p. 1521.

[29] T. L. Hill, S. A. Neild, and D. J. Wagg, "Comparing the direct normal form method with harmonic balance and the method of multiple scales," *Procedia engineering*, vol. 199, pp. 869–874, 2017.